Performance and Delay Analysis of Hybrid ARQ With Incremental Redundancy Over Double Rayleigh Fading Channels

Ali Chelli, *Member, IEEE*, Emna Zedini, Mohamed-Slim Alouini, *Fellow, IEEE*, John R. Barry, *Senior Member, IEEE*, and Matthias Pätzold, *Senior Member, IEEE*

Abstract—In this paper, we study the performance of hybrid automatic repeat request (HARQ) with incremental redundancy over double Rayleigh channels, a common model for the fading amplitude of vehicle-to-vehicle communication systems. We investigate the performance of HARQ from an information theoretic perspective. Analytical expressions are derived for the ϵ-outage capacity, the average number of transmissions, and the average transmission rate of HARQ with incremental redundancy assuming a maximum number of HARQ rounds. Moreover, we evaluate the delay experienced by Poisson arriving packets for HARQ with incremental redundancy. We provide analytical expressions for the expected waiting time, the packet's sojourn time in the queue, the average consumed power, and the energy efficiency. In our study, the communication rate per HARQ round is adjusted to the average signal-to-noise ratio (SNR) such that a target outage probability is not exceeded. This setting conforms with communication systems in which a quality of service is expected regardless of the channel conditions. Our analysis underscores the importance of HARQ in improving the spectral efficiency and reliability of communication systems. We demonstrate as well that the explored HARQ scheme achieves full diversity. Additionally, we investigate the tradeoff between energy efficiency and spectral efficiency.

Index Terms—Hybrid automatic repeat request (HARQ), incremental redundancy, energy efficiency, delay analysis, information outage capacity, average transmission rate, average number of transmissions.

I. INTRODUCTION

IN recent years, there is a growing interest in vehicle-to-vehicle (V2V) communication systems. Such systems provide mobility support and a wide range of applications aiming to reduce the number of road accidents and to improve the traffic flow. To cope with the problems faced during the development and performance investigation of future V2V communication systems, a solid knowledge of the underlying multipath fading channel characteristics is essential. Measurement results in [1] have shown that if vehicles are driving in the middle lanes of highways or in an urban environment, then the double-bounce scattering components caused by fixed scatterers are dominant. The double-bounce scattering mechanism has been assumed in several V2V channel models, such as the two-ring model [2], the street model [3], and the T-junction street model [4]. Under double-bounce scattering conditions, the fading amplitude is modeled as a double Rayleigh process [5], which can be expressed as a product of two independent Rayleigh processes. The double Rayleigh channel is more severe than the classical Rayleigh channel [6]. Therefore, the performance of communication systems over double Rayleigh channels needs to be studied carefully.

In vehicular environments, the wireless channel experiences fast fading variations caused by the high mobility of the transmitter, the receiver, and the scatterers. Under such conditions, the channel's coherence time is too short to allow for a feedback of the instantaneous channel gain from the receiver to the transmitter. In absence of channel state information (CSI) at the transmitter, power and rate adaptation schemes become impossible yielding a significant drop in the channel capacity. To cope with this problem, the hybrid automatic repeat request (HARQ) mechanism provides a promising solution.

HARQ combines automatic repeat request and forward error correction [7]. The data packet is first protected using channel coding techniques and then transmitted. The receiver sends an ACK (NACK) message to indicate successful (unsuccessful) reception. If the data packet is received correctly, the transmitter sends the next data packet. Otherwise, new sequences belonging to the same data packet are sent. For HARQ with incremental redundancy (IR), the transmitter sends new parity bits in each HARQ round. The receiver decodes the data packet based on all HARQ rounds. For a given data packet, the transmission terminates when successful decoding occurs at the receiver or a maximum number M of rounds is reached. A detailed description of the HARQ scheme with IR is provided in [8, Sec. II]. The number of HARQ rounds required to transmit an error-free data packet varies according to the channel conditions. Therefore, the amount of information sent through the channel

is adapted implicitly to the link quality even in absence of CSI at the transmitter. This feature makes HARQ very attractive, especially for fast fading channels, such as V2V channels.

In our investigation, we consider a double Rayleigh block fading channel, where the fading is assumed constant for one HARQ round and independent for different HARQ rounds. In the following, we present arguments supporting the block fading channel assumption. Firstly, each HARQ round corresponds to one transmission time slot. In V2V communications, the time slot duration is typically less than 0.8 ms. In this case, the channel can be considered constant during the whole time slot duration. In fact, V2V measurements at 5.9 GHz [9], [10] showed that the 90% coherence time equals to 1 ms for suburban environments.[1] Secondly, in practice, subsequent HARQ rounds are separated by few time slots to provide the destination node with enough time for decoding and feedback (ACK/NACK). As a result, we can assume that the channel realizations are independent for subsequent HARQ rounds. It follows that the assumption of block fading channel is reasonable.

Much of the prior work on HARQ focuses on code design and performance analysis. A high-rate code can be constructed from a low-rate code by puncturing the parity bits. The transmission starts with a high-rate code. Additional redundancy bits are sent whenever necessary. Different error correction codes can be used in this scheme, such as convolutional codes [11], [12] and low-density parity-check (LDPC) codes [13], [14]. The performance of HARQ in terms of throughput and error probability over Rayleigh channels have been investigated in [15], [16]. The author of [17] investigated the expected waiting time and the sojourn time of packets in the buffer for the case of cooperative truncated HARQ.

Very few papers have focused on information theoretic aspects of HARQ. In [18], the authors derive a relationship between HARQ throughput and mutual information. In [19] the authors assume multiple relay nodes, the best relay node is first determined using a distributed algorithm. The selected relay cooperates with the source to transmit the message to the destination. The performance of the communication system is analyzed with emphasis on the outage probability and the delay-limited throughput. The authors of [19] assume that the channel is constant during all the HARQ rounds. In [8], the performance of different HARQ schemes over relay channels is explored considering that the channel realizations are different for subsequent HARQ rounds as opposed to [19]. For a given outage probability, it is shown in [20] that in case of Rayleigh block fading channels, HARQ allows to communicate at a higher rate compared to systems without HARQ.

In this paper, we investigate the performance of HARQ with IR over double Rayleigh channels, as opposed to the classical Rayleigh channel. In our study, the data rate per HARQ round is adjusted to the average signal-to-noise ratio (SNR) such that a target outage probability is achieved. This is as opposed to [17] where a constant transmission rate is considered. Our main contributions can be summarized as follows. We provide

analytical expressions for the average number of transmissions, the ϵ-outage capacity, and the average transmission rate for HARQ with IR. This is in contrast to [21] which focuses on the performance of HARQ with code combining. We show that even in absence of CSI at the transmitter, the HARQ with IR rate is close to the ergodic capacity after some few rounds. We compare the average transmission rate of HARQ to the rate achieved without HARQ. We demonstrate that systems with HARQ have a significant advantage compared to systems without HARQ.

The additional contributions of this paper compared to our paper [22] consist of analyzing the delay performance, studying the energy efficiency, and investigating the diversity order of HARQ with IR over double Rayleigh channels. Analytical expressions are derived for the average waiting time for a data packet (the average time elapsed between the first packet transmission and the packet arrival) and the average sojourn time in the buffer (the average waiting time in the buffer for a data packet before the start of its transmission). We study as well the energy efficiency of the HARQ scheme and explore the tradeoff between energy efficiency and spectral efficiency. Finally, we investigate the diversity order of the HARQ scheme and show that it can achieve full diversity.

The remainder of the paper is organized as follows. In Section II, we investigate the performance of HARQ with IR over double Rayleigh channels. We perform a mutual-information-based analysis of HARQ. Analytical solutions are provided for the ϵ-outage capacity, the average number of transmissions, and the average transmission rate. Section III presents the delay model and provides the exact expression for the second-order moment of the number of transmissions. In Section IV, the energy efficiency is explored and an analytical expression for the average consumed power is derived. The diversity order of the system is determined in Section V. The derived analytical expressions are numerically evaluated and illustrated in Section VI. Finally, Section VII provides some concluding remarks.

II. HARQ WITH IR

A. System Model

When using HARQ with IR, the transmission starts with a high-rate code. A small number of parity bits is transmitted with the information bits in the first HARQ round. If decoding fails, the transmitter sends new parity bits. At the receiver side, the parity bits received during all HARQ rounds are combined, which results in a lower coding rate. Thus, the coding rate is implicitly adapted to the channel conditions. The lowest coding rate corresponds to the case when the maximum number of M HARQ rounds are used for the transmission of a given data packet. The capacity in bits/symbol of HARQ with IR after m rounds can be expressed as

$$C_m = \frac{1}{m} \sum_{i=1}^{m} \log_2(1 + \gamma_s \gamma_i), \qquad (1)$$

---

[1]The authors of [10] define the 90% coherence time as the time interval over which the fading remains constant with a probability of 0.9.

where γ_s denotes the SNR, while γ_i is the squared envelop of the channel gain during the ith transmission round. The random variables γ_i $(i = 1, \ldots, M)$ are independent and identically distributed (i.i.d.). In case of double Rayleigh fading, the PDF of γ_i is given by [5]

$$p_{\gamma_i}(x) = \frac{2}{\bar{\gamma}} K_0\left(2\sqrt{\frac{x}{\bar{\gamma}}}\right), \qquad (2)$$

where $\bar{\gamma}$ is the mean value of γ_i, while $K_0(\cdot)$ is the modified Bessel function of zeroth order [23].

It is worth mentioning that the number of retransmissions can vary from one data packet to another depending on the channel conditions. If the channel conditions are good, a single HARQ round could be sufficient for error-free decoding. In the case of bad channel conditions, M HARQ rounds might be required to transmit one data packet. Thus, the transmission rate needs to be defined in a proper way. Towards this aim, let us assume that the transmitted data packet contains b information bits. In each HARQ round, L symbols are transmitted. The transmission rate of the first HARQ round in bits per channel use can be written as $R_1 = b/L$. Note that the transmission rate varies depending on the number of HARQ rounds used to transmit a data packet. The transmission rate is equal to $R_m = R_1/m$, if m HARQ rounds are used to transmit one data packet. We denote by Q_n the number of HARQ rounds required for an error-free transmission of the nth data packet. The average transmission rate for N data packets can be expressed as

$$\overline{R} = \frac{Nb}{L \sum\limits_{n=1}^{N} Q_n} = \frac{R_1}{\frac{1}{N}\sum\limits_{n=1}^{N} Q_n} = \frac{R_1}{\mathbb{E}(T_r)}, \qquad (3)$$

with $\mathbb{E}(\cdot)$ denoting the expectation operator and $\mathbb{E}(T_r)$ being the average number of transmissions per data packet.

The expression in (3) is valid for the case where there is no delay constraint, i.e., $M \to \infty$. However, if M is finite the transmission of a data packet may fail after M rounds. This event is called an outage event. The communication system is in outage if the capacity C_M is less than the rate R_M. Hence, an outage occurs if the accumulated mutual information after M rounds is less than the rate R_1. The outage probability of HARQ with IR after M rounds reads as

$$P_{\text{out}}^{\text{IR},M}(R_1) = \mathbb{P}\left\{\sum_{m=1}^{M} \log_2(1 + \gamma_s\gamma_m) \leqslant R_1\right\}. \qquad (4)$$

Note that for $M \to \infty$ the outage probability $P_{\text{out}}^{\text{IR},M}(R_1)$ becomes equal to zero and the average transmission rate $\overline{R}$ reduces to the expression provided in (3). However, for a finite value of M, the outage probability is nonzero and the average transmission rate can be determined as

$$\overline{R} = \frac{R_1\left(1 - P_{\text{out}}^{\text{IR},M}(R_1)\right)}{\mathbb{E}(T_r)}. \qquad (5)$$

A similar expression of the average transmission rate has been provided in [24]. From (5), one can conclude that if we choose a large value of R_1 the outage probability after M HARQ rounds

is approximately one and the average transmission rate $\overline{R}$ in (5) tends to zero. To avoid such a situation, we have to maintain the outage probability under a certain threshold ϵ and choose the rate R_1 subject to this threshold ϵ.

B. Outage Analysis and Average Transmission Rate

1) Approximate Analysis: The ϵ-outage capacity C_ϵ^M after M rounds is defined in [25] as the largest transmission rate R_1, such that the outage probability $P_{\text{out}}^{\text{IR},M}(R_1) \leqslant \epsilon$. In the case of HARQ with IR, the ϵ-outage capacity C_ϵ^M is obtained by solving the equation

$$P_{\text{out}}^{\text{IR},M}\left(C_\epsilon^M\right) = \epsilon. \qquad (6)$$

We set the rate of the first HARQ round as $R_1 = C_\epsilon^M$. In this way, we guarantee that the outage probability is equal to ϵ after M HARQ rounds. A fixed outage probability is guaranteed for any SNR level. The average transmission rate $C_\epsilon^{\text{IR},M}$ of HARQ with IR can be obtained using (5) as

$$C_\epsilon^{\text{IR},M} = \frac{C_\epsilon^M\left(1 - P_{\text{out}}^{\text{IR},M}\left(C_\epsilon^M\right)\right)}{\mathbb{E}(T_r)} = \frac{C_\epsilon^M(1-\epsilon)}{\mathbb{E}(T_r)}. \qquad (7)$$

The expression of the average number of transmissions $\mathbb{E}(T_r)$ with a maximum number of rounds M can be expressed similarly to [17, Eq. (18)] as

$$\mathbb{E}(T_r) = 1 + \sum_{m=1}^{M-1} P(F^1, \ldots, F^m), \qquad (8)$$

where F^m denotes the event decoding failure after m HARQ rounds. The probability $P(F^1, \ldots, F^m)$ of a transmission failure after m rounds decreases as m increases. This probability is equal to the outage probability after m HARQ rounds. It follows,

$$\begin{aligned}
P(F^1, \ldots, F^m) &= P_{\text{out}}^{\text{IR},m}(R_1) = P_{\text{out}}^{\text{IR},m}(C_\epsilon^M) \\
&= \mathbb{P}\left\{\sum_{i=1}^{m} \log_2(1 + \gamma_s\gamma_i) \leqslant C_\epsilon^M\right\} \\
&= F_{\zeta_m}\left(C_\epsilon^M\right),
\end{aligned} \qquad (9)$$

where $F_{\zeta_m}(x)$ is the cumulative distribution function (CDF) of $\zeta_m = \sum_{i=1}^{m} \log_2(1 + \gamma_s\gamma_i)$. Note that ζ_m is the accumulated mutual information of HARQ with IR after m rounds. To determine the probability of a transmission failure after m rounds, we need an expression of the CDF $F_{\zeta_m}(x)$ as well as the expression of the ϵ-outage capacity C_ϵ^M of HARQ with IR. An approximate solution for the CDF $F_{\zeta_m}(x)$ is derived in Appendix A, where it is shown that $F_{\zeta_m}(x)$ can be written as

$$F_{\zeta_m}(x) \approx \Gamma_{\alpha_{\zeta_m}+1}\left(\frac{x}{\beta_{\zeta_m}}\right), \qquad (10)$$

with $\Gamma_a(\cdot)$ being the incomplete gamma function [23, Eq. (6.5.1)]. The terms α_{ζ_m} and β_{ζ_m} are functions of the SNR and their expressions are provided in Appendix A. The

ϵ-outage capacity of HARQ with IR C_ϵ^M can be obtained by solving (6) as

$$\epsilon = \mathbb{P}\left\{ \sum_{m=1}^{M} \log_2(1 + \gamma_s\gamma_m) \leqslant C_\epsilon^M \right\}$$

$$\approx \Gamma_{\alpha_{\zeta_M}+1}\left(\frac{C_\epsilon^M}{\beta_{\zeta_M}}\right). \tag{11}$$

It follows that for HARQ with IR, the ϵ-outage capacity C_ϵ^M can be written as

$$C_\epsilon^M \approx \beta_{\zeta_M}\Gamma_{\alpha_{\zeta_M}+1}^{-1}(\epsilon), \tag{12}$$

where $\Gamma_a^{-1}(\cdot)$ denotes the inverse of the incomplete gamma function $\Gamma_a(\cdot)$. Hence, by using (8)–(10) and (12), the average number of transmissions can be expressed as

$$\mathbb{E}(T_r) \approx 1 + \sum_{m=1}^{M-1} \Gamma_{\alpha_{\zeta_m}+1}\left(\frac{C_\epsilon^M}{\beta_{\zeta_m}}\right)$$

$$\approx 1 + \sum_{m=1}^{M-1} \Gamma_{\alpha_{\zeta_m}+1}\left(\frac{\beta_{\zeta_M}}{\beta_{\zeta_m}}\Gamma_{\alpha_{\zeta_M}+1}^{-1}(\epsilon)\right). \tag{13}$$

Note that the average number of transmissions $\mathbb{E}(T_r)$ of HARQ with IR is a function of SNR. However, for systems without HARQ, the average number of transmissions is constant and equals to $\mathbb{E}(T_r) = M$. In fact, for HARQ, the transmission stops when the accumulated mutual information is sufficient for successful decoding at the receiver. This is equivalent to adaptive coding. Actually, for a given packet, M HARQ rounds at maximum can be used. Under good channel conditions, successful decoding is possible after $m(m < M)$ rounds.

For systems that do not use HARQ and in absence of CSI at the transmitter, it is not possible to do rate adaptation. The solution that will be adopted in this case is to transmit always M sequences since we do not have CSI at the transmitter. Under such conditions, the transmitter considers the worst case scenario (bad channel conditions) for which M sequences are required to decode successfully a data packet. When using M transmissions for all data packets (systems without HARQ), we are encoding b information bits into $M \times L$ symbols which yields a constant coding rate of $b/(M \cdot L)$. This is as opposed to HARQ where the number of retransmissions for a given data packet is adapted to the channel conditions thanks to the feedback mechanism.

After substituting (12) and (13) in (7), we can express the average transmission rate $C_\epsilon^{\text{IR},M}$ of HARQ with IR as

$$C_\epsilon^{\text{IR},M} \approx \frac{\beta_{\zeta_M}\Gamma_{\alpha_{\zeta_M}+1}^{-1}(\epsilon)(1-\epsilon)}{1 + \sum_{m=1}^{M-1}\Gamma_{\alpha_{\zeta_m}+1}\left(\frac{\beta_{\zeta_M}}{\beta_{\zeta_m}}\Gamma_{\alpha_{\zeta_M}+1}^{-1}(\epsilon)\right)}. \tag{14}$$

The transmission rate without HARQ can be obtained as

$$C_\epsilon^{\text{No-HARQ},M} \approx \frac{\beta_{\zeta_M}\Gamma_{\alpha_{\zeta_M}+1}^{-1}(\epsilon)(1-\epsilon)}{M}. \tag{15}$$

Since the average number of transmissions $\mathbb{E}(T_r)$ in (13) is less than M, it follows that the average transmission rate $C_\epsilon^{\text{IR},M}$ of HARQ with IR is larger than the average transmission rate $C_\epsilon^{\text{No-HARQ},M}$ without HARQ.

2) High SNR Approximation: In this section, we derive an expression for the average transmission rate $C_\epsilon^{\text{IR},M}$ of HARQ with IR for the case of high SNR. The expression of $C_\epsilon^{\text{IR},M}$ in (14) has been obtained by approximating the PDF of ζ_m with a gamma distribution. At high SNR, a closed-form solution can be found for the average transmission rate $C_\epsilon^{\text{IR},M}$ of HARQ with IR, the ϵ-outage capacity C_ϵ^M after M rounds, and the average number of transmissions $\mathbb{E}(T_r)$. The term C_ϵ^M is obtained by solving the equation

$$\epsilon = P_{\text{out}}^{\text{IR},M}\{R_1\} = P_{\text{out}}^{\text{IR},M}\{C_\epsilon^M\}$$

$$= \mathbb{P}\left\{\sum_{m=1}^{M}\log_2(1+\gamma_s\gamma_m) \leqslant C_\epsilon^M\right\}$$

$$= \mathbb{P}\left\{\sum_{m=1}^{M}\log_2(\gamma_s) + \log_2\left(\frac{1}{\gamma_s}+\gamma_m\right) \leqslant C_\epsilon^M\right\}$$

$$\underset{\gamma_s \gg 1}{\approx} \mathbb{P}\left\{M\log_2(\gamma_s) + \sum_{m=1}^{M}\log_2(\gamma_m) \leqslant C_\epsilon^M\right\}$$

$$= \mathbb{P}\left\{\log_2\left(\prod_{m=1}^{M}\gamma_m\right) \leqslant C_\epsilon^M - M\log_2(\gamma_s)\right\}$$

$$= \mathbb{P}\left\{\prod_{m=1}^{M}\gamma_m \leqslant 2^{C_\epsilon^M - M\log_2(\gamma_s)}\right\}. \tag{16}$$

Let $F_{\xi_M}(x)$ denote the CDF of the product of M squared double Rayleigh processes given as $\xi_M = \prod_{m=1}^{M}\gamma_m$. The exact expression of the CDF $F_{\xi_M}(x)$ is derived in Appendix B. The ϵ-outage capacity C_ϵ^M after M rounds can be expressed as

$$C_\epsilon^M \underset{\gamma_s \gg 1}{\approx} M\log_2(\gamma_s) + \log_2\left(F_{\xi_M}^{-1}(\epsilon)\right), \tag{17}$$

where $F_{\xi_M}^{-1}(\cdot)$ stands for the inverse of the CDF $F_{\xi_M}(\cdot)$ of ξ_M. The expression of the average number of transmissions $\mathbb{E}(T_r)$ is given by (8). Under the high SNR assumption, the probability of a transmission failure for HARQ with IR after m rounds can be expressed as

$$P(F^1,\ldots,F^m) = P_{\text{out}}^{\text{IR},m}(R_1) = P_{\text{out}}^{\text{IR},m}(C_\epsilon^M)$$

$$= \mathbb{P}\left\{\sum_{i=1}^{m}\log_2(1+\gamma_s\gamma_i) \leqslant C_\epsilon^M\right\}$$

$$\underset{\gamma_s \gg 1}{\approx} \mathbb{P}\left\{\prod_{i=1}^{m}\gamma_i \leqslant 2^{C_\epsilon^M - m\log_2(\gamma_s)}\right\}$$

$$= F_{\xi_m}\left(2^{C_\epsilon^M - m\log_2(\gamma_s)}\right)$$

$$= F_{\xi_m}\left(\gamma_s^{M-m}F_{\xi_M}^{-1}(\epsilon)\right). \tag{18}$$

By using (7), (8), (17), and (18), the average transmission rate $C_\epsilon^{\mathrm{IR},M}$ of HARQ with IR can be written at high SNR as

$$C_\epsilon^{\mathrm{IR},M} \underset{\gamma_s \gg 1}{\approx} \frac{\left(M \log_2(\gamma_s) + \log_2\left(F_{\xi_M}^{-1}(\epsilon) \right) \right)(1-\epsilon)}{1 + \sum_{m=1}^{M-1} F_{\xi_m}\left(\gamma_s^{M-m} F_{\xi_M}^{-1}(\epsilon) \right)}. \quad (19)$$

III. DELAY MODEL

To control the flow of the packets in the network, we consider that the source is equipped with a buffer to store the packets before transmission. We assume Poisson arriving packets at the buffer with arrival rate λ. The waiting time for a data packet corresponds to the time elapsed between the first sequence transmission and the successful decoding of the packet at the destination. The average waiting time for a data packet can be evaluated using the Pollaczek-Khinchin equation [26]

$$W = \frac{\lambda \mathbb{E}\left(T_r^2 \right) T_F^2}{2(1-\rho)} + \frac{T_F}{2}, \quad (20)$$

where T_F is the frame duration. The parameter ρ should satisfy the following stability condition

$$\rho = \lambda \mathbb{E}(T_r) T_F < 1. \quad (21)$$

The packet's sojourn time in the buffer is [26]

$$T_{\mathrm{soj}} = W + \mathbb{E}(T_r) T_F. \quad (22)$$

The expression of the average number of transmissions $\mathbb{E}(T_r)$ is provided by (13). The second-order moment $\mathbb{E}(T_r^2)$ of the total number of transmissions is derived in Appendix C as

$$\mathbb{E}\left(T_r^2 \right) = 1 + \sum_{m=1}^{M-1} (2m+1) P(F^1, \ldots, F^m)$$

$$\approx 1 + \sum_{m=1}^{M-1} (2m+1) \Gamma_{\alpha_{\zeta_m}+1}\left(\frac{C_\epsilon^M}{\beta_{\zeta_m}} \right). \quad (23)$$

IV. ENERGY EFFICIENCY

During the past decades, system designers have focused their efforts on the enhancement of the spectral efficiency of communication systems. Towards this aim, many advanced communication techniques have been utilized, such as orthogonal frequency-division multiple access (OFDMA), multiple-input multiple-output (MIMO) techniques, and cooperative communications. However, with the explosive growth in network throughput, more and more energy is consumed in wireless networks. In the context of energy limited resources and green communications, the notion of energy-efficient communication have been paid increasing attention [27]–[29]. In [27], energy efficiency of HARQ with IR for two-way relay systems with network coding has been studied. A literature survey on energy efficiency is provided in [29].

In this section, we study the energy efficiency[2] of HARQ with IR over double Rayleigh channels. The energy efficiency, denoted by η_{EE}, is defined as the ratio of the throughput and the average consumed power and is given by [28], [29]

$$\eta_{EE} = \frac{C_\epsilon^M (1-\epsilon)}{\bar{P}}, \quad (24)$$

where C_ϵ^M is the ϵ-outage capacity. The quantity $\bar{P}$ stands for the average consumed power, which can be determined for the HARQ scheme as

$$\bar{P} = P \cdot P(S^1) + 2P \cdot P(F^1, S^2) + \ldots + (M-1)P$$

$$\cdot P(F^1, \ldots, S^{M-1}) + MP \cdot P(F^1, \ldots, F^{M-1})$$

$$= P \cdot \mathbb{E}(T_r) = P \cdot \left(1 + \sum_{m=1}^{M-1} \Gamma_{\alpha_{\zeta_m}+1}\left(\frac{C_\epsilon^M}{\beta_{\zeta_m}} \right) \right). \quad (25)$$

The term P stands for the consumed power per HARQ round. We denote by $P(S^1)$ the probability of successful transmission in the first round, while $P(F^1, \ldots, S^{M-1})$ refers to the probability of a transmission failure in the 1st, 2nd, $\ldots$, $M-2$th HARQ rounds and a success at $M-1$th round. If only one transmission round is used to transmit the data packet (the probability of occurrence of this event is $P(S^1)$), the amount of consumed power would be equal to P. If two transmission rounds are utilized to transmit one data packet (the probability of this event is $P(F^1, S^2)$), the amount of consumed power would be equal to $2P$. We would consume an amount of power equal to MP if a transmission failure occurs at round $M-1$ (the probability of this event is $P(F^1, \ldots, F^{M-1})$). The average consumed power is obtained by summing up all the possible values of consumed power weighted by the probability of occurrence of such event. The result in (25) shows that we can express the average consumed power as the product of two terms: the power P consumed per HARQ round and the average number of transmissions $\mathbb{E}(T_r)$. Using (25), we can express the energy efficiency as

$$\eta_{EE} = \frac{C_\epsilon^M (1-\epsilon)}{P \left(1 + \sum_{m=1}^{M-1} \Gamma_{\alpha_{\zeta_m}+1}\left(\frac{C_\epsilon^M}{\beta_{\zeta_m}} \right) \right)} = \frac{C_\epsilon^{\mathrm{IR},M}}{P}. \quad (26)$$

A. Quasiconcavity and Maximization of the Energy Efficiency

In this section, we prove the quasiconcavity of the energy efficiency and provide a method for determining the optimal power yielding maximum energy efficiency.

The energy efficiency $\eta_{EE}(P)$ is the ratio of the spectral efficiency $C_\epsilon^{\mathrm{IR},M}(P)$ and the power P as shown in (26). Proving the quasiconcavity of $\eta_{EE}(P)$ is equivalent to prove the quasiconvexity of $-\eta_{EE}(P)$. To this end, we make use of the following theorem [30].

Theorem 1: Let $g(x)$ and $f(x)$ be defined on a convex set C such that $f(x) \neq 0$ for all $x \in C$. Then, $g(x)/f(x)$ is

---

[2]The unit of energy efficiency is bits per Joule.

quasiconvex on C if $f(x)$ is either linear or convex on C and $g(x) \leq 0$ for all $x \in C$.

For our case, we substitute the function $f(x)$ with P which is linear and nonzero. Additionally, we replace the function $g(x)$ with $-C_\epsilon^{\text{IR},M}(P)$ which is nonpositive for all $P \in (0,\infty)$. Notice also that the interval $(0,\infty)$ is a convex set. Consequently, based on **Theorem 1** the function $-\eta_{EE}(P)$ is quasiconvex and hence $\eta_{EE}(P)$ is quasiconcave.

Since $\eta_{EE}(P)$ is quasiconcave, it follows that there exist a point P^* below which the energy efficiency is nondecreasing (i.e., increasing or constant) and above which the energy efficiency is nonincreasing (i.e., decreasing or constant), where the point P^* is a global maximizer of the energy efficiency.[3]

Moreover, the energy efficiency tends to zero as $P \to \infty$. This can be proven using the following inequalities

$$C_\epsilon^{\text{IR},M}(P) \leq \bar{C} = \mathbb{E}\left\{\log_2(1 + \gamma_s\gamma)\right\} \qquad (27)$$

$$\leq \log_2\left(1 + \gamma_s\mathbb{E}\{\gamma\}\right). \qquad (28)$$

The inequality in (27) comes from the fact that the outage capacity is upper bounded by the ergodic capacity $\bar{C}$. In (28), we exploited Jensen's inequality and the fact that $\log_2(x)$ is a concave function. Hence, we can obtain the following upper bound on the energy efficiency as $P \to \infty$

$$\lim_{P \to \infty} \eta_{EE} = \lim_{P \to \infty} \frac{C_\epsilon^{\text{IR},M}(P)}{P}$$

$$\leq \lim_{P \to \infty} \frac{\log_2\left(1 + \gamma_s\mathbb{E}\{\gamma\}\right)}{P} = 0. \qquad (29)$$

On one hand, $\lim_{P \to \infty} \eta_{EE} \leq 0$. On the other hand, $\eta_{EE} \geq 0$ then $\lim_{P \to \infty} \eta_{EE} \geq 0$. As a result, $\lim_{P \to \infty} \eta_{EE} = 0$.

Note that the quasiconcavity of $\eta_{EE}(P)$ proves the existence of a global maximum. In the following, we explain how the solution that maximizes the energy efficiency can be computed.

Maximizing the energy efficiency $\eta_{EE}(P)$ is equivalent to minimizing $-\eta_{EE}(P)$. The quasiconvex optimization problem can be written as

$$\begin{array}{ll} \underset{P}{\text{minimize}} & -\eta_{EE}(P) \\ \text{subject to} & -P < 0, \end{array} \qquad (30)$$

where $-\eta_{EE}(P)$ is quasiconvex and the inequality constraint is linear. Solving the quasiconvex optimization problem in (30) can be reduced to solving a sequence of convex optimization problems [31]. A general approach to quasiconvex optimization is based on the representation of the sublevel sets of a quasiconvex function via a family of convex inequalities [31]. To this end, we need to construct a family of convex function ϕ_t which satisfy

$$-\eta_{EE}(P) \leq t \iff \phi_t(P) \leq 0. \qquad (31)$$

Note that $\phi_t(P)$ should be convex with respect to (w.r.t.) P and decreasing w.r.t. t.

[3]This is a definition of quasiconcavity which holds for real continuous functions as it is the case of the spectral efficiency which is continuous and real valued.
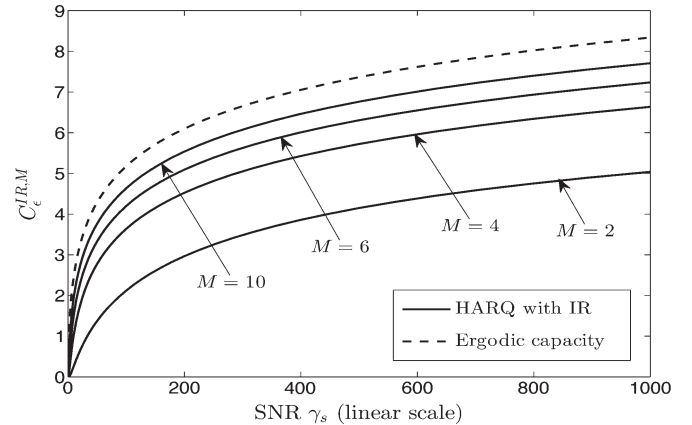

Fig. 1.   Spectral efficiency $C_\epsilon^{\text{IR},M}$ versus SNR in linear scale.

We can construct this function as

$$\phi_t(P) = -C_\epsilon^{\text{IR},M}(P) - tP, \qquad (32)$$

where t is a nonnegative real number. For $\phi_t(P)$ to be convex w.r.t. P, we only need to prove that $-C_\epsilon^{\text{IR},M}(P)$ is a convex function[4] of P. This is equivalent to prove the concavity of the spectral efficiency $C_\epsilon^{\text{IR},M}$ w.r.t. the SNR in linear scale. This fact is confirmed numerically from Fig. 1, but is hard to prove analytically due to the complicated expression of the spectral efficiency[5] $C_\epsilon^{\text{IR},M}$. Since the spectral efficiency is concave (as shown numerically in Fig. 1) then $-C_\epsilon^{\text{IR},M}(P)$ is a convex function w.r.t. P. On the other hand, the function P is linear and strictly positive function. Consequently, for each P, $\phi_t(P)$ in (32) is decreasing in t and for each t, $\phi_t(P)$ is convex w.r.t. P.

Let P^* denote the optimal value of the quasiconvex problem in (30). If the feasibility problem

$$\begin{array}{ll} \text{find} & P \\ \text{subject to} & \phi_t(P) \leq 0 \\ & -P < 0 \end{array} \qquad (33)$$

is feasible, then $P^* \leq t$. Conversely, if the problem (33) is infeasible, then $P^* \geq t$. It is worth noting that the feasibility problem in (33) is convex since its inequality constraints are convex. Thus, it is possible to solve the convex feasibility problem in (33) for each value of t and find out whether it is feasible or not. To determine the optimal value P^*, we start with an interval $[l, u]$ known to contain P^*. Then we solve the feasibility problem (33) at the midpoint, i.e., for $t = (l + u)/2$. If the problem (33) is feasible for $t = (l + u)/2$ then $P^* \in [l, t]$. If the problem (33) is unfeasible for $t = (l + u)/2$ then $P^* \in [t, u]$. In a second step we apply the same procedure to the interval obtained from the first step. This is repeated until the width of the interval is small enough. An algorithm using bisection and which solves a convex feasibility problem at each

[4]Here, we use the fact that the sum of a convex and linear function is convex.
[5]Note that it is possible to prove that the ergodic capacity (which has a similar trend as the spectral efficiency $C_\epsilon^{\text{IR},M}$) is concave w.r.t. SNR in linear scale. This can be shown by computing the second derivative of the ergodic capacity. The numerical evaluation of the second derivative reveals that this function is always negative which proves that the ergodic capacity is concave.

step can be found in [31, pp. 146]. A similar algorithm can be used to determine the optimal solution P^*.

In Fig. 12, we plot the energy efficiency versus the power $\tilde{P}$ ($\tilde{P} = 10 \log_{10}(P)$). This figure shows that the energy efficiency is a quasiconcave function of $\tilde{P}$. This fact can be proven by showing the quasiconvexity of $-\eta_{EE}(\tilde{P})$ w.r.t. $\tilde{P}$ using **Theorem 1**. The quasiconcavity of $\eta_{EE}(\tilde{P})$ explains the shape of the energy efficiency, plotted in Fig. 12, which increases for low values of the power $\tilde{P}$ then decreases for medium and high values of $\tilde{P}$. The optimal value $\tilde{P}^*$ which maximizes $\eta_{EE}(\tilde{P})$ can be determined as $\tilde{P}^* = 10 \log_{10}(P^*)$.

B. Tradeoff Between Energy Efficiency and Spectral Efficiency

We notice that the spectral efficiency and the energy efficiency cannot be improved simultaneously, meaning that a tradeoff has to be found between energy efficiency and spectral efficiency of HARQ with IR over double Rayleigh channels. If we fix the values of ϵ, M, and the noise power, then the spectral efficiency increases if we increase the transmitted power per round P [see Fig. 3]. However, the energy efficiency increases as P increases up to a certain value P^* that maximizes the energy efficiency [see Fig. 12]. If the power $P > P^*$ the energy efficiency starts decreasing while the spectral efficiency keeps increasing. Thus for values of $P \leq P^*$ both the energy efficiency and the spectral efficiency can be increased together, whereas $P > P^*$ we experience a tradeoff between energy efficiency and spectral efficiency, i.e., we cannot improve both quantities simultaneously. The impact of the maximum number M of HARQ rounds on this tradeoff is investigated in more detail in Section VI-C.

V. DIVERSITY ORDER OF THE HARQ SCHEME

In this section, we investigate the performance of HARQ with IR over double Rayleigh channels. We show in the following that the HARQ scheme can achieve full diversity. The diversity order d of a transmission scheme is defined as [32]

$$d = -\lim_{\gamma_s \to \infty} \frac{\ln(P_e)}{\ln(\gamma_s)}, \qquad (34)$$

where P_e is the error probability. If a capacity achieving code is utilized, then the probability of error is well approximated by the information outage probability $P_{\text{out}}^M(C_\epsilon^M)$ [33]. At high SNR, this information outage probability can be determined as

$$P_{\text{out}}\left(C_\epsilon^M\right) = \mathbb{P}\left\{\sum_{i=1}^{M} \log_2(1 + \gamma_s \gamma_i) \leqslant C_\epsilon^M\right\}$$

$$\underset{\gamma_s \gg 1}{\approx} \mathbb{P}\left\{\prod_{i=1}^{M} \gamma_i \leqslant \frac{2^{C_\epsilon^M}}{\gamma_s^M}\right\} = F_{\xi_M}\left(\frac{2^{C_\epsilon^M}}{\gamma_s^M}\right)$$

$$= G_{1,2M+1}^{2M,1}\left[\frac{2^{C_\epsilon^M}}{(\gamma_s\bar{\gamma})^M} \,\middle|\, \begin{matrix} 1 \\ 1, \ldots, 0 \end{matrix}\right], \qquad (35)$$

where $G_{p,q}^{m,n}(\cdot)$ is the Meijer's G-function defined in (A.4).

To compute the diversity order of the HARQ scheme, we need to compute the series expansion of the function in (35) as $\gamma_s \to \infty$. This is equivalent to computing the series expansion of the function $f(x) = G_{1,2M+1}^{2M,1}\left[x \,\middle|\, \begin{matrix} 1 \\ 1, \ldots, 1, 0 \end{matrix}\right]$ as $x \to 0$, where $x = 2^{C_\epsilon^M}/(\gamma_s\bar{\gamma})^M$. For any value of M, it can be shown using the series expansion of $f(x)$ as $x \to 0$ that $f(x)$ can be approximated as

$$f(x) \approx -x(\ln x)^{2M-1} + o(x^2) \qquad \forall M, \qquad (36)$$

where the notation $o(x^2)$ implies that the term $o(x^2)$ vanishes as $x \to 0$. Using the results in (36) and utilizing the change of variable $x = 2^{C_\epsilon^M}/(\gamma_s\bar{\gamma})^M$, we get an approximation at high SNR for the outage probability for different values of M as

$$P_e = P_{\text{out}}\left(C_\epsilon^M\right) \underset{\gamma_s \to \infty}{\approx} -\frac{2^{C_\epsilon^M}}{(\gamma_s\bar{\gamma})^M} \ln\left(\frac{2^{C_\epsilon^M}}{(\gamma_s\bar{\gamma})^M}\right)^{2M-1}. \qquad (37)$$

To determine the diversity order, we first compute the term $\ln(P_e)$ which can be approximated at high SNR as

$$\ln(P_e) \underset{\gamma_s \to \infty}{\approx} \ln\left(\frac{2^{C_\epsilon^M}}{(\gamma_s\bar{\gamma})^M}\right) + \ln\left[-(2M-1)\ln\left(\frac{2^{C_\epsilon^M}}{(\gamma_s\bar{\gamma})^M}\right)\right]$$

$$= \ln\left(2^{C_\epsilon^M}\right) - M\left[\ln(\gamma_s) + \ln(\bar{\gamma})\right] + \ln(2M-1)$$

$$+ \ln\left(M\left[\ln(\gamma_s) + \ln(\bar{\gamma})\right] - \ln\left(2^{C_\epsilon^M}\right)\right). \qquad (38)$$

Applying the definition of the diversity order in (34), we obtain

$$d = -\lim_{\gamma_s \to \infty} \frac{\ln(P_{qe})}{\ln(\gamma_s)}$$

$$\overset{(a)}{=} -\lim_{\gamma_s \to \infty} \frac{\ln\left(2^{C_\epsilon^M}\right)}{\ln(\gamma_s)} + \lim_{\gamma_s \to \infty} \frac{M\ln(\gamma_s)}{\ln(\gamma_s)}$$

$$+ \lim_{\gamma_s \to \infty} \frac{M\ln(\bar{\gamma})}{\ln(\gamma_s)} - \lim_{\gamma_s \to \infty} \frac{\ln(2M-1)}{\ln(\gamma_s)}$$

$$- \lim_{\gamma_s \to \infty} \frac{\ln\left(M\left[\ln(\gamma_s) + \ln(\bar{\gamma})\right] - \ln(2^{C_\epsilon^M})\right)}{\ln(\gamma_s)}$$

$$\overset{(b)}{=} \lim_{\gamma_s \to \infty} \frac{M\ln(\gamma_s)}{\ln(\gamma_s)} = M. \qquad (39)$$

In (b), we have used the fact that all the terms in (a) tend to zero as $\gamma_s \to \infty$ except the term $M\ln(\gamma_s)/\ln(\gamma_s)$ which tends to M as $\gamma_s \to \infty$. Thus, the diversity order d of the HARQ scheme is equal to M.

VI. NUMERICAL RESULTS

A. Average Transmission Rate

In this section, the analytical expressions for the average number of transmissions and the average transmission rate are evaluated numerically and illustrated. In our analysis, since there is no closed-form expression for the CDF $F_{\zeta_m}(x)$ of the accumulated mutual information ζ_m, we approximate this CDF $F_{\zeta_m}(x)$ by the CDF of a gamma distribution [see (10)]. To show the accuracy of this approximation, we illustrate in Fig. 2 the
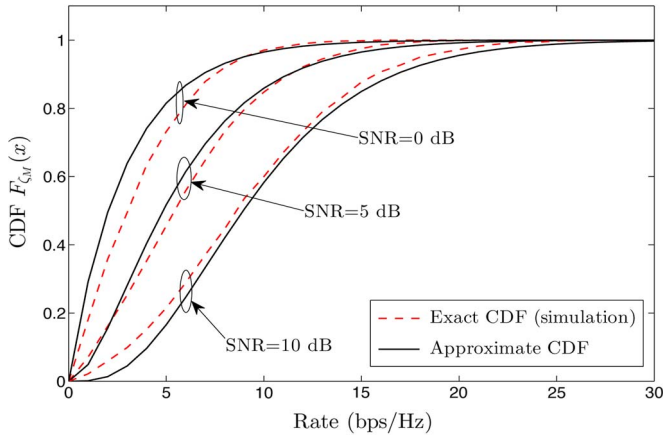
Fig. 2. Exact and approximate CDF of the accumulated mutual information $\zeta_M = \sum_{i=1}^{M} \log_2(1 + \gamma_s \gamma_i)$ for $M = 4$ at SNR = 0, 5, and 10 dB.
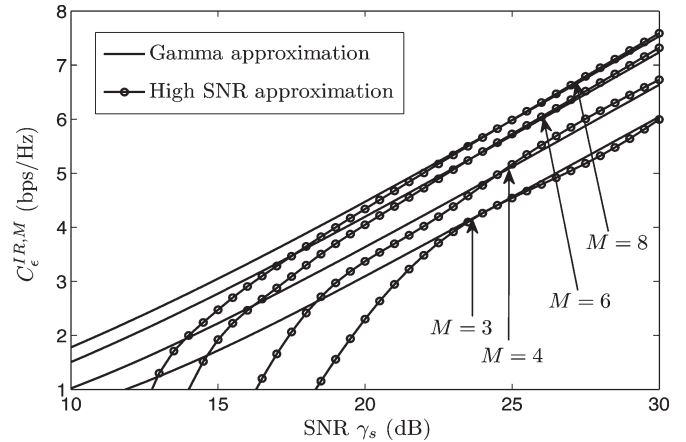

Fig. 4. Gamma approximation and high SNR approximation of the average transmission rate $C_\epsilon^{\mathrm{IR},M}$ of HARQ with IR for $\epsilon = 0.01$.
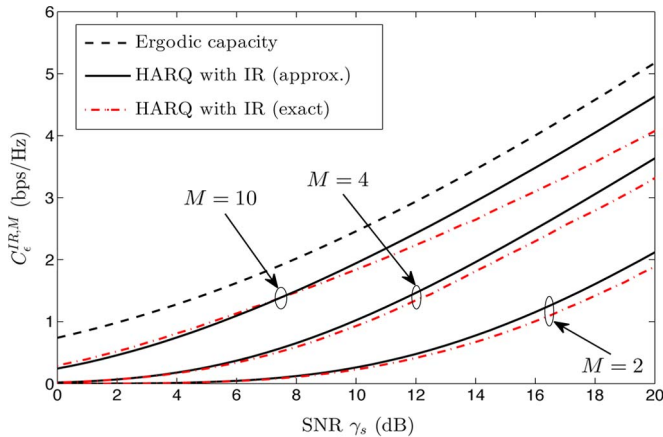

Fig. 3. Exact and approximate average transmission rate $C_\epsilon^{\mathrm{IR},M}$ of HARQ with IR for $\epsilon = 0.01$.
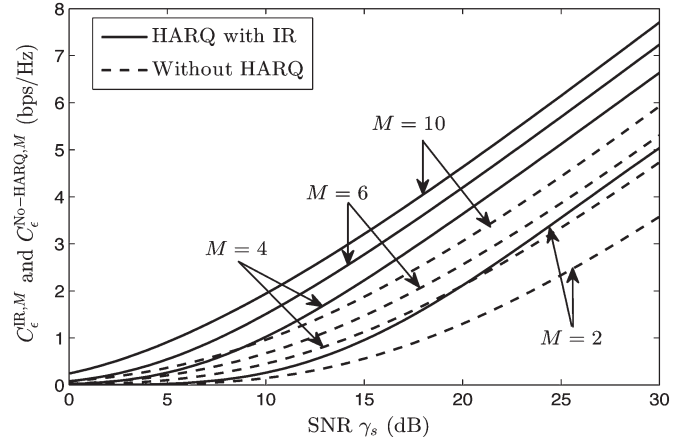

Fig. 5. Average transmission rate $C_\epsilon^{\mathrm{IR},M}$ of HARQ with IR and the rate without HARQ $C_\epsilon^{\mathrm{No-HARQ},M}$ for $\epsilon = 0.01$.

exact CDF of ζ_m obtained via Monte Carlo simulations together with the gamma approximation of the CDF of ζ_m. The results in Fig. 2 have been obtained for SNR = 0, 5, and 10 dB and for a value of $M = 4$. The gamma approximation becomes more tight as the SNR increases. Numerical results in Fig. 2 show that the gamma approximation is reasonably accurate for the range of interest for the rate R_1 and SNR parameters. Besides, this approximation yields important insights.

In Fig. 3, the average transmission rate $C_\epsilon^{\mathrm{IR},M}$ of HARQ with IR is plotted for $\epsilon = 0.01$. It can be seen from this figure that $C_\epsilon^{\mathrm{IR},M}$ increases as M and the SNR increase. It is well known that the ergodic capacity can only be achieved in the idealized setting where the CSI at the transmitter is available. The HARQ scheme allows to have adaptive rate without the need of CSI at the transmitter. From Fig. 3, it can be seen that after few HARQ rounds, the average transmission rate $C_\epsilon^{\mathrm{IR},M}$ becomes close to the ergodic capacity even in the absence of CSI at the transmitter. Additionally, in Fig. 3 the exact average transmission rate (obtained via Monte Carlo simulations) and the approximate average transmission rate (determined using gamma approximation) are illustrated. From this figure it can be seen that the gamma approximation is fairly accurate for $M = 2$ and 4 for all SNR values. For $M = 10$, the gamma

approximation is accurate up to an SNR of 12 dB. As the value of M increases the accuracy reduces especially at high SNR. However, the level of accuracy remains reasonable. The maximum error that we perceive is in the order of 0.5 bps/Hz for $M = 10$ and an SNR of 20 dB, which is a reasonably small error. It is worth mentioning that for practical systems typical values of M are in the order of 4. A value of $M = 10$ would generally be considered to be large in practice since it leads to a large delay. This shows that the gamma approximation is quite accurate for the range of interest of M.

In (19), an analytical expression has been derived for the average transmission rate $C_\epsilon^{\mathrm{IR},M}$ at high SNR for the case of HARQ with IR. Under the assumption of high SNR, it is possible to obtain the exact solutions for the PDF and CDF of ξ_m which allows to get an approximate solution for the average transmission rate in (19). To validate the result in (19), we compare it to the average transmission rate $C_\epsilon^{\mathrm{IR},M}$ in (14) obtained using the gamma approximation of the PDF of the process ζ_m. In Fig. 4, both results for the average transmission rate are illustrated. A good fitting can be seen between both expressions at high SNR for different values of M.

In Fig. 5, we illustrate the average transmission rate $C_\epsilon^{\mathrm{IR},M}$ in (14) of HARQ with IR and the rate $C_\epsilon^{\mathrm{No-HARQ},M}$ without
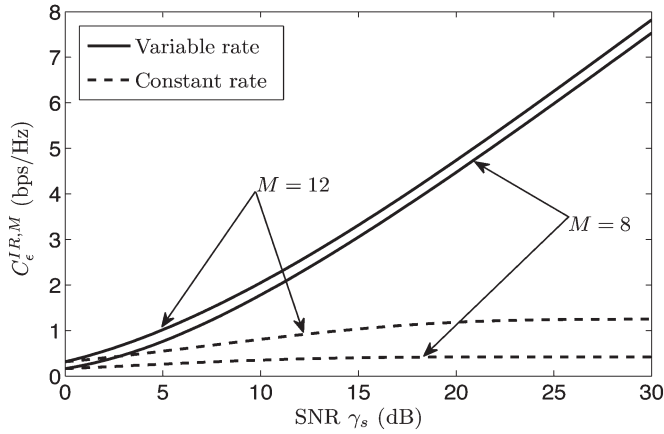
Fig. 6. Average transmission rate $C_\epsilon^{\text{IR},M}$ of HARQ with IR for the cases of variable and constant rate schemes for $\epsilon = 0.01$.

HARQ [see (15)]. It can be seen from this figure that HARQ with IR provides a significant improvement in the transmission rate relatively to systems without HARQ. For the same value of M, we observe at low SNR that the advantage of using HARQ with IR is limited. On the contrary, in the high SNR regime, a significant improvement in the rate can be observed if HARQ with IR is used. For instance, for an SNR of 30 dB, a gain of 2 bps/Hz can be achieved by using HARQ with IR and setting the value of M to 4. In fact, at high SNR, the average number of transmissions for a given packet is less than M. Actually, for good channel conditions the mutual information accumulated over few HARQ rounds is sufficient for successful decoding at the receiver. However, in absence of CSI at the transmitter, a fixed rate is used for systems without HARQ. Consequently, even under good channel conditions, M rounds are required to transmit one data packet. The gain achieved using HARQ with IR increases as the SNR increases. In absence of CSI at the transmitter, we are obliged to use a fixed rate which makes the communication system nonadaptive and a loss in the mutual information is observed. With HARQ, implicit rate adaptation is possible, even in the absence of CSI. Notice that some few HARQ rounds make the gap to the ergodic capacity reasonably small.

In Figs. 3–5, we consider a variable rate per HARQ round. Under this setting, the rate is adjusted to the average SNR such that a target outage probability ϵ is not exceeded. In Fig. 6, we explore the effect of the transmission rate R_1 per HARQ round on the average transmission rate $C_\epsilon^{\text{IR},M}$. Towards this aim, we compare the performance of a scheme with a variable rate and a scheme with a constant rate. For the latter scheme, the rate R_1 per round is the same for all SNR values and equal to the variable rate for an SNR of 0 dB, i.e., $R_1 = C_\epsilon^M$ (0 dB). In this way, we ensure that the target outage probability ϵ is maintained for the constant rate scheme for any SNR larger than 0 dB, since the outage probability decreases with the SNR value.

The average transmission rate $C_\epsilon^{\text{IR},M}$ is illustrated in Fig. 6 for the cases of constant rate and variable rate schemes. It can be seen from this figure that the use of a variable rate improves the system throughput. For instance, for an SNR of 30 dB and for $\epsilon = 0.01$, we can achieve in case of $M = 8$ a gain of 6.6 bps/Hz in the average transmission rate if we adjust the rate per
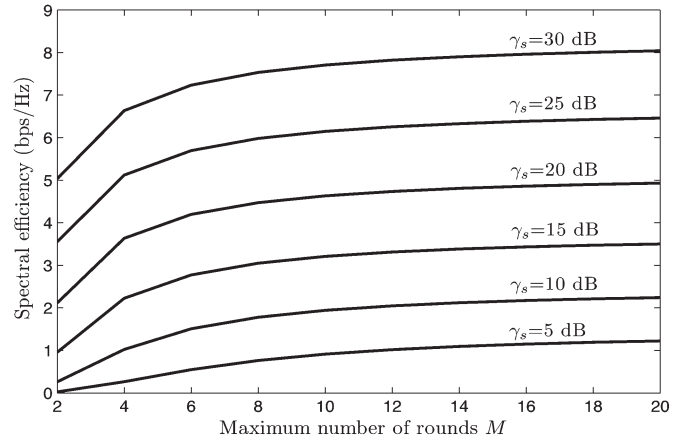

Fig. 7. Spectral efficiency $C_\epsilon^{\text{IR},M}$ of HARQ with IR versus the maximum number of rounds M.
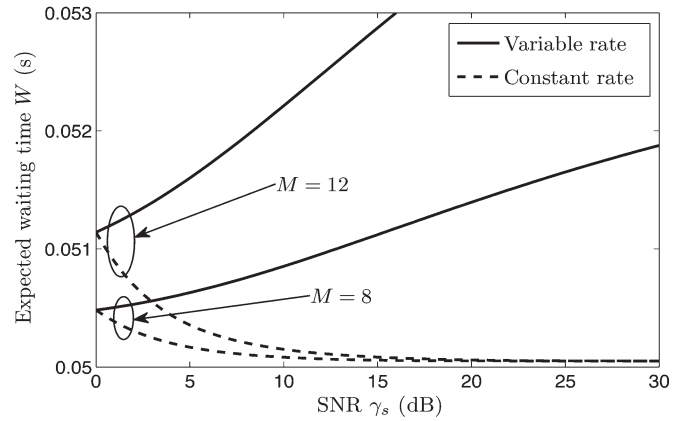

Fig. 8. Expected waiting time W of packets of HARQ with IR for variable rate and constant rate schemes.

HARQ round to the average SNR (variable rate) compared to the constant rate scheme. It is also shown in Fig. 6 that the throughput increases as M increases for both schemes (constant and variable rate).

Fig. 7 presents the plots of the spectral efficiency[6] $C_\epsilon^{\text{IR},M}$ of HARQ with IR versus the maximum number of rounds M for different SNR values. This figure underscores the impact of M on the spectral efficiency. It can be noticed from Fig. 7 that a large gain in spectral efficiency is obtained if we increase M from 2 to 4. This gain increases as the SNR increases. For instance, increasing M from 2 to 4, yields a spectral efficiency gain of 2 bps/Hz and 1.2 bps/Hz for an SNR of 30 dB and 10 dB, respectively. For values of $M \geqslant 6$, an increase in the value of M does not lead to a significant improvement in the spectral efficiency regardless of the SNR value.

B. Delay Results

In this section, the analytical expressions for the average waiting time W and sojourn time T_{soj} are numerically evaluated and illustrated for both variable rate and constant rate schemes. We set the frame length to $T_F = 1$ s. In Figs. 8 and 9,

---

[6]The terms average transmission rate and spectral efficiency are used interchangeably throughout the paper.
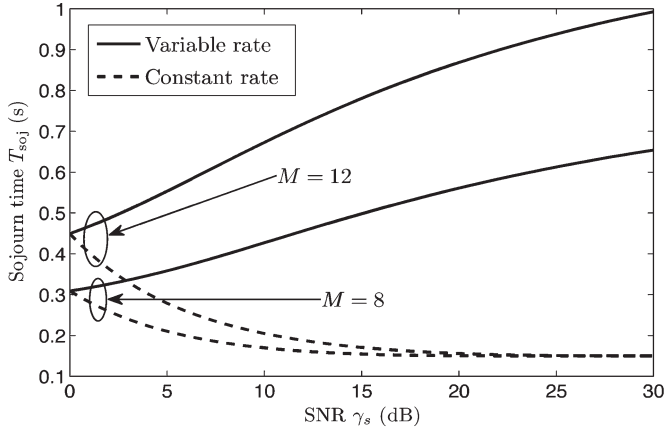
Fig. 9. Packet's sojourn time T_{soj} in the network of queues of HARQ with IR for variable rate and constant rate schemes.
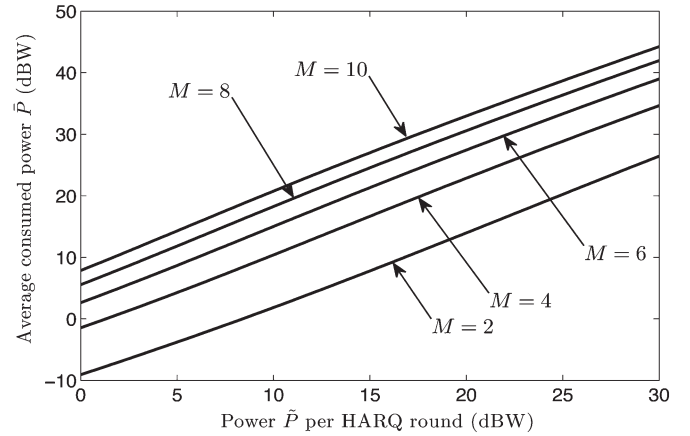

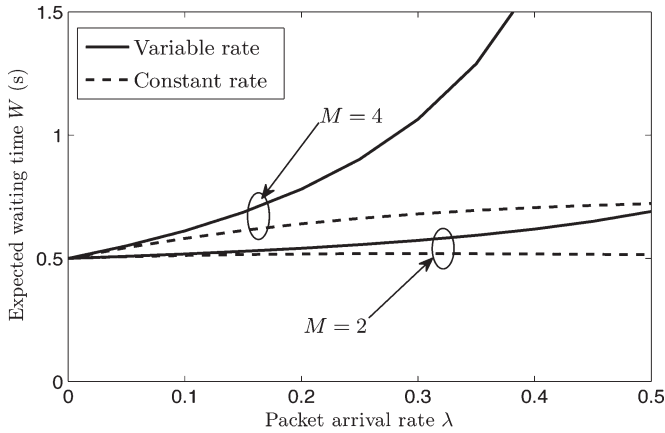Fig. 11. Average consumed power $\bar{P}$ of HARQ with IR versus power per HARQ round.

Fig. 10. Expected waiting time W of packets of HARQ with IR versus the packet arrival rate λ for variable rate and constant rate schemes.
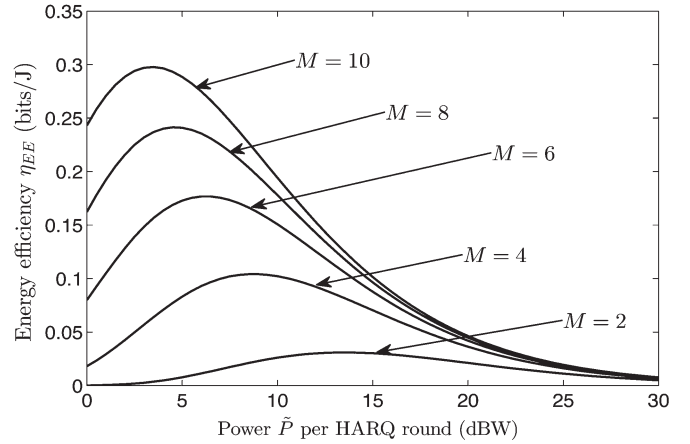

Fig. 12. Energy efficiency η_{EE} of HARQ with IR versus power per HARQ round.

respectively, we depict the expected waiting time and the sojourn time versus the SNR γ_s for $M = 8$ and 12. The packet arrival rate is set to $\lambda = 0.01$.

We notice that the use of a constant rate allows decreasing the expected waiting time and the sojourn time compared to the case of variable rate. Actually, the constant rate scheme has a smaller rate per round than the variable rate scheme and consequently a smaller number of retransmissions. It is worth mentioning that there is a tradeoff between spectral efficiency and the delay experienced by a transmitted data packet. It can be observed in Figs. 6, 8, and 9 that the variable rate scheme achieves a large throughput at the expense of a larger waiting and sojourn time. On the other hand, the constant rate scheme leads to a small throughput but allows decreasing the expected waiting time and sojourn time of the packet in the queue. It can be seen in Figs. 8 and 9 that the expected waiting time and the sojourn time increases as M increases either we utilize a constant or a variable rate scheme.

In Fig. 10, we illustrate the expected waiting time W versus the packet arrival rate λ for $M = 2$ and 4. From this figure, we notice that the average waiting time W increases as the packet arrival rate λ increases. Moreover, the constant rate scheme is less sensitive to an increase of M compared to the variable rate scheme. In fact, for $\lambda = 0.5$, the increase of M from 2 to

4 leads to a significant increase in the expected waiting time W for the variable rate scheme. Under the same conditions, a slight change in the expected waiting time is experienced for the constant rate scheme.

C. Average Consumed Power and Energy Efficiency

This section is devoted to the study of the average consumed power $\bar{P}$, the energy efficiency η_{EE}, and the tradeoff between spectral efficiency $C_\epsilon^{\text{IR},M}$ and energy efficiency η_{EE}. Fig. 11 shows the variation of the average consumed power $\bar{P}$ as a function of the power $\tilde{P}$ per HARQ round for different values of M. It can be observed from this figure that the average consumed power $\bar{P}$ increases as $\tilde{P}$ and M increase. Note that the graphs in Fig. 11 are plotted in the log-log scale. The fact that the curves of $\bar{P}$ versus $\tilde{P}$ are very well approximated by affine equations confirms that the following equation holds $\bar{P} \approx aP^b$, where b corresponds to the slope of the curve and a is the $\bar{P}$ value corresponding to $P = 1$ Watt. We recall that $\tilde{P} = 10\log_{10}(P)$.

The energy efficiency η_{EE} as a function of the power $\tilde{P}$ per HARQ round is illustrated in Fig. 12 for different values of M. It can be seen that the energy efficiency η_{EE} is a quasiconcave function of the power $\tilde{P}$ as discussed in Section IV-A. The
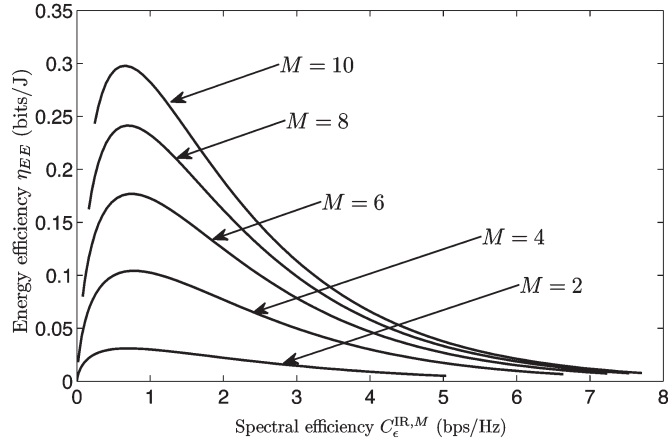
Fig. 13. Tradeoff between energy efficiency η_{EE} and spectral efficiency $C_\epsilon^{\mathrm{IR},M}$.

energy efficiency increases for small values of the power $\tilde{P}$ then decreases for medium values of the power $\tilde{P}$. The energy efficiency tends to zero as $\tilde{P} \to \infty$.

For a given value of M, the energy efficiency curve versus power $\tilde{P}$ shows that the energy efficiency exhibits a single maximum at $\tilde{P}^*$. A bisection method for computing $\tilde{P}^*$ is presented in Section IV-A. By setting $\tilde{P} = \tilde{P}^*$, it is guaranteed that the system operates at the optimal point that maximizes the energy efficiency. It can be noticed from Fig. 12 that the optimal operating power $\tilde{P}^*$ per HARQ round decreases as the value of M increases. Additionally, the maximum achievable energy efficiency increases as M increases. For instance, the maximum energy efficiency can be improved by a factor of 15 if we increase the value of M from 2 to 10.

In Fig. 13, we plot the energy efficiency η_{EE} as a function of the spectral efficiency $C_\epsilon^{\mathrm{IR},M}$ for different values of M. From Fig. 13, we notice that both the energy efficiency and the spectral efficiency can be increased together if the target spectral efficiency does not exceed 0.8 bps/Hz. The spectral efficiency cannot be increased beyond this value without a loss in the energy efficiency. Hence, there is a tradeoff between energy efficiency and spectral efficiency. By varying the rate per HARQ round, we can quantify this tradeoff which is illustrated in Fig. 13. It can also be observed from Fig. 13 that both the energy efficiency and the spectral efficiency increase as M increases.

VII. CONCLUSION

In this paper, we have investigated the performance of HARQ with IR over double Rayleigh channels. In our analysis, we have adjusted the transmission rate to the average SNR such that a fixed target outage probability is not exceeded. We have provided analytical expressions for the average number of transmissions, the ϵ-outage capacity, and the average transmission rate. We demonstrate that even in the absence of CSI at the transmitter, the rate of HARQ with IR becomes close to the ergodic capacity after few rounds. This feature makes HARQ very attractive, especially for fast fading channels such as V2V channels. In fact, for such channels, the coherence time is too short to allow for a feedback of the instantaneous

channel conditions to the transmitter. We compared the average transmission rate of HARQ with IR to the rate achieved without HARQ. Supported by our analysis, we are convinced that HARQ provides a significant advantage compared to systems without HARQ.

We have derived analytical expressions of the expected waiting time and the sojourn time of packets in the buffer for the cases of variable and constant rate per HARQ round. Our numerical study of the average waiting time and the sojourn time highlighted the existence of a tradeoff between these quantities and the spectral efficiency. We have also studied the impact of the maximum number of rounds on the average waiting time and the sojourn time and observed that increasing M yields an increase in the delay. Additionally, we have demonstrated that the explored HARQ scheme achieves full diversity. Finally, our analysis underscore the tradeoff between energy efficiency and spectral efficiency.

APPENDIX A
APPROXIMATE SOLUTION FOR THE PDF AND THE CDF OF THE ACCUMULATED MUTUAL INFORMATION ζ_m

We denote by ζ_m the accumulated mutual information of HARQ with IR after m rounds given as $\zeta_m = \sum_{i=1}^m \log_2(1 + \gamma_s \gamma_i)$. In this appendix, we derive an approximate solution for the PDF and the CDF of ζ_m. Using Laguerre series [34], the PDF of ζ_m can be approximated as

$$p_{\zeta_m}(x) \approx p_0^{\zeta_m}(x) = \frac{x^{\alpha_{\zeta_m}}}{\beta_{\zeta_m}^{(\alpha_{\zeta_m}+1)}\Gamma(\alpha_{\zeta_m}+1)} \exp\left(-\frac{x}{\beta_{\zeta_m}}\right),$$

(A.1)

where $\alpha_{\zeta_m} = ([\mathbb{E}(\zeta_m)]^2/\mathrm{Var}(\zeta_m)) - 1$, $\beta_{\zeta_m} = \mathrm{Var}(\zeta_m)/\mathbb{E}(\zeta_m)$, and $\Gamma(\cdot)$ is the gamma function. To determine the parameters α_{ζ_m} and β_{ζ_m}, we need to derive the mean value and the variance of the process ζ_m. Since the processes γ_i are i.i.d., the following equality holds $\mathbb{E}(\zeta_m) = \sum_{i=1}^m \mathbb{E}\{\log_2(1 + \gamma_s \gamma_i)\} = m\mathbb{E}\{\log_2(1 + \gamma_s \gamma)\}$. The term $\mathbb{E}\{\log_2(1 + \gamma_s \gamma)\}$ is equal to the ergodic capacity $\bar{C}$ of the double Rayleigh channel which can be written as

$$\bar{C} = \int_0^\infty \log_2(1 + \gamma_s \gamma) p_\gamma(\gamma) d\gamma$$

$$= \int_0^\infty \log_2(e) \ln(1 + \gamma_s \gamma) \frac{2}{\bar{\gamma}} K_0\left(2\sqrt{\frac{\gamma}{\bar{\gamma}}}\right) d\gamma \quad \text{(A.2)}$$

$$= \frac{\log_2(e)}{\gamma_s \bar{\gamma}} G_{1,3}^{3,1}\left[\frac{1}{\gamma_s \bar{\gamma}} \middle| \begin{matrix} -1 \\ -1, -1, 0 \end{matrix}\right], \quad \text{(A.3)}$$

where $G_{p,q}^{m,n}(\cdot)$ is the Meijer's G-function defined as [35]

$$G_{p,q}^{m,n}\left(z \middle| \begin{matrix} a_1, \ldots, a_p \\ b_1, \ldots, b_q \end{matrix}\right)$$
$$= \frac{1}{j2\pi} \int_{\mathcal{C}} \frac{\prod_{i=1}^m \Gamma(b_i + s) \prod_{i=1}^n \Gamma(1 - a_i - s)}{\prod_{i=n+1}^p \Gamma(a_i + s) \prod_{i=m+1}^q \Gamma(1 - b_i - s)} z^{-s} ds.$$

(A.4)

It has to be noted that the result in (A.3) is obtained as follows. First, we substitute in (A.2) the zeroth order modified Bessel function $K_0(\cdot)$ and the logarithm function by their Meijer's G-representations in [36, Eq. (03.04.26.0008.01)] and [36, Eq. (01.04.26.0003.01)], respectively. Second, using [36, Eq. (07.34.21.0013.01)], we obtain after some algebraic manipulations the result in (A.3).

The variance of the process ζ_m can be expressed as

$$\mathrm{Var}(\zeta_m) = \sum_{i=1}^{m} \mathrm{Var}\left(\{\log_2(1+\gamma_s\gamma_i)\}\right)$$
$$= m\left\{\mathbb{E}\left\{(\log_2(1+\gamma_s\gamma))^2\right\} - \mathbb{E}\{\log_2(1+\gamma_s\gamma)\}^2\right\},$$
$$\tag{A.5}$$

where

$$\mathbb{E}\left\{[\log_2(1+\gamma_s\gamma)]^2\right\}$$
$$= \int_0^\infty [\log_2(1+\gamma_s\gamma)]^2 \frac{2}{\bar\gamma} K_0\left(2\sqrt{\frac{\gamma}{\bar\gamma}}\right) d\gamma$$
$$= (\log_2(e))^2 \int_0^\infty [\ln(1+\gamma_s\gamma)]^2 \frac{2}{\bar\gamma} K_0\left(2\sqrt{\frac{\gamma}{\bar\gamma}}\right) d\gamma$$
$$= (\log_2(e))^2 I(\gamma). \tag{A.6}$$

We evaluate the integral $I(\gamma)$ using integration by parts, namely

$$\int_0^\infty u\, dv = \lim_{\gamma\to\infty}(uv) - \lim_{\gamma\to 0}(uv) - \int_0^\infty v\, du. \tag{A.7}$$

First, let $u = (\ln(1+\gamma_s\gamma))^2$. Thus $du = 2\ln(1+\gamma_s\gamma)(\gamma_s d\gamma/(1+\gamma_s\gamma))$. Then, let $dv = (2/\bar\gamma)K_0(2\sqrt{\gamma/\bar\gamma})$. Hence, $v = -2\sqrt{\gamma/\bar\gamma}K_1(2\sqrt{\gamma/\bar\gamma})$. The first two terms in (A.7) are equal to zero. It follows,

$$I(\gamma) = \int_0^\infty 4\sqrt{\frac{\gamma}{\bar\gamma}} K_1\left(2\sqrt{\frac{\gamma}{\bar\gamma}}\right) \frac{\ln(1+\gamma_s\gamma)}{\frac{1}{\gamma_s}+\gamma} d\gamma$$
$$\underset{\gamma_s\gg 1}{\approx} \int_0^\infty \frac{4}{\gamma}\sqrt{\frac{\gamma}{\bar\gamma}} K_1\left(2\sqrt{\frac{\gamma}{\bar\gamma}}\right) \ln(1+\gamma_s\gamma)\, d\gamma \tag{A.8}$$
$$= 2G_{1,3}^{3,1}\left[\frac{1}{\gamma_s\bar\gamma}\bigg|\begin{matrix}0\\0,0,0\end{matrix}\right]. \tag{A.9}$$

It is worth mentioning that the expression in (A.9) is obtained from (A.8) by using the same steps utilized to reach the result in (A.3) from (A.2).

After determining the mean value and the variance of the process ζ_m, the parameters α_{ζ_m} and β_{ζ_m} can be computed and an expression of the PDF can be obtained using (A.1). The CDF of ζ_m can be deduced as

$$F_{\zeta_m}(x) \approx F_0^{\zeta_m}(x) = \int_0^x p_0^{\zeta_m}(z)dz$$
$$= \Gamma_{\alpha_{\zeta_m}+1}\left(\frac{x}{\beta_{\zeta_m}}\right). \tag{A.10}$$

APPENDIX B
PDF AND CDF OF THE PRODUCT OF SQUARED DOUBLE RAYLEIGH PROCESSES ξ_m

In this appendix, we derive an expression for the PDF and the CDF of the product of squared double Rayleigh processes $\xi_m = \prod_{i=1}^m \gamma_i = \prod_{i=1}^m \gamma_{1,i}\gamma_{2,i}$, where $\gamma_{1,i}$ and $\gamma_{2,i}$ are i.i.d. squared Rayleigh processes. The processes $\gamma_{1,i}$ and $\gamma_{2,i}$ are exponentially distributed and have the same mean value, i.e., $\bar\gamma_{1,i} = \bar\gamma_{2,i} = \sqrt{\bar\gamma_i} = \sqrt{\bar\gamma}$. In [37], the inverse Mellin transform has been used to derive the PDF of the product of Rayleigh processes. We use the same method to derive the PDF for the product of squared double Rayleigh processes. The PDF of ξ_m is obtained as the inverse Mellin transform of $\rho_h = \mathbb{E}\{(\xi_m)^h\}$, defined by the contour integral

$$p_{\xi_m}(x) = \frac{1}{j2\pi} \int_{\mathcal{C}} \rho_h x^{-(h+1)} dh. \tag{B.1}$$

The term ρ_h can be expressed as

$$\rho_h = \mathbb{E}\left\{(\xi_m)^h\right\} = \prod_{i=1}^m \mathbb{E}\left\{\gamma_i^h\right\} = \prod_{i=1}^{2m} \mathbb{E}\left\{\gamma_{1,i}^h\right\}, \tag{B.2}$$

where

$$\mathbb{E}\{\gamma_{1,i}^h\} = \int_0^\infty \frac{x^h}{\sqrt{\bar\gamma}}\exp\left(-\frac{x}{\sqrt{\bar\gamma}}\right)dx. \tag{B.3}$$

Using the change of variable $u = x/\sqrt{\bar\gamma}$, we can write

$$\mathbb{E}\{\gamma_{1,i}^h\} = (\sqrt{\bar\gamma})^h \int_0^\infty u^h\exp(-u)du = (\sqrt{\bar\gamma})^h\Gamma(h+1). \tag{B.4}$$

It follows $\rho_h = \bar\gamma^{hm}[\Gamma(h+1)]^{2m}$. Substituting ρ_h in (B.1) and setting $s = h+1$, we can express the PDF $p_{\xi_m}(x)$ as

$$p_{\xi_m}(x) = \frac{1}{j2\pi}\int_{\mathcal{C}} \bar\gamma^{hm}[\Gamma(h+1)]^{2m} x^{-(h+1)} dh$$
$$= \frac{1}{j2\pi}\int_{\mathcal{C}} \bar\gamma^{m(s-1)}[\Gamma(s)]^{2m} x^{-s} ds$$
$$= \frac{1}{\bar\gamma^m}\frac{1}{j2\pi}\int_{\mathcal{C}} [\Gamma(s)]^{2m}\left(\frac{x}{\bar\gamma^m}\right)^{-s} ds$$
$$= \frac{1}{\bar\gamma^m}G_{0,2m}^{2m,0}\left[\frac{x}{\bar\gamma^m}\bigg|\begin{matrix}\\0,\dots,0\end{matrix}\right]. \tag{B.5}$$

The CDF $F_{\xi_m}(x)$ of the process ξ_m can be deduced from the PDF $p_{\xi_m}(x)$ as

$$F_{\xi_m}(x) = \int_0^x p_{\xi_m}(z)dz$$
$$= \frac{1}{\bar\gamma^m}\frac{1}{j2\pi}\int_{\mathcal{C}} [\Gamma(s)]^{2m}\int_0^x\left(\frac{z}{\bar\gamma^m}\right)^{-s} dz\, ds$$
$$= \frac{x}{\bar\gamma^m}\frac{1}{j2\pi}\int_{\mathcal{C}} \frac{[\Gamma(s)]^{2m}}{1-s}\left(\frac{x}{\bar\gamma^m}\right)^{-s} ds. \tag{B.6}$$

Using the relation $1 - s = \Gamma(2 - s)/\Gamma(1 - s)$, we obtain

$$
\begin{aligned}
F_{\xi_m}(x) &= \frac{x}{\bar{\gamma}^m} G_{1,2m+1}^{2m,1} \left[\frac{x}{\bar{\gamma}^m} \, \middle| \, \begin{matrix} 0 \\ 0, \ldots, 0, -1 \end{matrix} \right] \\
&= G_{1,2m+1}^{2m,1} \left[\frac{x}{\bar{\gamma}^m} \, \middle| \, \begin{matrix} 1 \\ 1, \ldots, 1, 0 \end{matrix} \right].
\end{aligned} \tag{B.7}
$$

APPENDIX C
SECOND-ORDER MOMENT OF THE NUMBER OF TRANSMISSIONS

In this appendix, we derive the expression of the second-order moment of the number of transmissions T_r per data packet.

For a maximal number of rounds M, T_r is a discrete random variable that takes values in $\{1, \ldots, m, \ldots, M\}$:

- $T_r = 1$, if the transmission of the data packet succeeds in the first round. The probability of this event is denoted by $P(S^1)$, whereas the probability of the complimentary event (i.e., failure event after one HARQ round) is referred to as $P(F^1)$.
- $T_r = m$, if the transmission of the data packet fails in the first $m - 1$ rounds, and we have success in the mth round. The probability of this event is denoted by $P(F^1, \ldots, F^{m-1}, S^m)$, while $P(F^1, \ldots, F^{m-1}, F^m)$ stands for the probability of a transmission failure after m rounds.
- $T_r = M$, if the transmission of the data packet fails in the first $M - 1$ rounds, and we have either success or failure in the Mth transmission round.

Hence, the second-order moment of the number of transmissions per data packet reads as

$$
\mathbb{E}(T_r^2) = 1 P(S^1) + \sum_{m=2}^{M-1} m^2 P(F^1, \ldots, F^{m-1}, S^m) \\
+ M^2 P(F^1, \ldots, F^{M-1}). \tag{C.1}
$$

Utilizing the following identities

$$
P(S^1) = 1 - P(F^1) \tag{C.2}
$$
$$
\begin{aligned}
&P(F^1, \ldots, F^{m-1}, S^m) \\
&= P(F^1, \ldots, F^{m-1}) - P(F^1, \ldots, F^m),
\end{aligned} \tag{C.3}
$$

we can simplify the of the expression of the second-order moment of the number of transmissions as

$$
\begin{aligned}
\mathbb{E}\left(T_r^2\right) &= 1 - P(F^1) \\
&+ \sum_{m=2}^{M-1} m^2 \left[P(F^1, \ldots, F^{m-1}) - P(F^1, \ldots, F^m) \right] \\
&+ M^2 P(F^1, \ldots, F^{M-1}) \\
&= 1 - P(F^1) - \sum_{m=2}^{M-1} m^2 P(F^1, \ldots, F^m) \\
&+ \sum_{m=2}^{M-1} m^2 P(F^1, \ldots, F^{m-1}) \\
&+ M^2 P(F^1, \ldots, F^{M-1}) \\
&= 1 - \sum_{m=1}^{M-1} m^2 P(F^1, \ldots, F^m)
\end{aligned}
$$

$$
\begin{aligned}
&+ \sum_{m=2}^{M} m^2 P(F^1, \ldots, F^{m-1}) \\
&= 1 - \sum_{m=1}^{M-1} m^2 P(F^1, \ldots, F^m) \\
&+ \sum_{m=1}^{M-1} (m+1)^2 P(F^1, \ldots, F^m) \\
&= 1 + \sum_{m=1}^{M-1} \left((m+1)^2 - m^2 \right) P(F^1, \ldots, F^m) \\
&= 1 + \sum_{m=1}^{M-1} (2m+1) P(F^1, \ldots, F^m). \tag{C.4}
\end{aligned}
$$

REFERENCES

[1] A. G. Zajić, G. L. Stüber, and T. G. Pratt, "Statistical modelling and experimental verification for wideband MIMO mobile-to-mobile channels," in *Proc. 15th Int. Conf. Telecommun.*, St. Petersburg, Russia, Jun. 2008, pp. 1–6.
[2] M. Pätzold, B. Hogstad, and N. Youssef, "Modeling, analysis, and simulation of MIMO mobile-to-mobile fading channels," *IEEE Trans. Wireless Commun.*, vol. 7, no. 2, pp. 510–520, Feb. 2008.
[3] A. Chelli and M. Pätzold, "The impact of fixed and moving scatterers on the statistics of MIMO vehicle-to-vehicle channels," in *Proc. IEEE 69th VTC Spring*, Barcelona, Spain, Apr. 2009, pp. 1–6.
[4] H. Zhiyi, C. Wei, Z. Wei, M. Pätzold, and A. Chelli, "Modelling of MIMO vehicle-to-vehicle fading channels in T-junction scattering environments," in *Proc. 3rd EuCAP*, Berlin, Germany, Mar. 2009, pp. 652–656.
[5] W. Wongtrairat and P. Supnithi, "Performance of digital modulation in double Nakagami-m fading channels with MRC diversity," *IEICE Trans. Commun.*, vol. E92-B, no. 2, pp. 559–566, Feb. 2009.
[6] J. Salo, H. M. El-Sallabi, and P. Vainikainen, "Impact of double-Rayleigh fading on system performance," in *Proc. 1st Int. Symp. Wireless Pervasive Comput.*, Jan. 2006, pp. 1–5.
[7] D. J. Costello, J. Hagenauer, H. Imai, and S. B. Wicker, "Applications of error-control coding," *IEEE Trans. Inf. Theory*, vol. 44, no. 6, pp. 2531–2560, Oct. 1998.
[8] A. Chelli and M.-S. Alouini, "On the performance of hybrid-ARQ with incremental redundancy and with code combining over relay channels," *IEEE Trans. Wireless Commun.*, vol. 12, no. 8, pp. 3860–3871, Aug. 2013.
[9] B. Fan, D. D. Stancil, and H. Krishnan, "Toward understanding characteristics of dedicated short range communications (DSRC) from a perspective of vehicular network engineers," in *Proc. 16th Annu. Int. Conf. MobiCom*, Sep. 2010, pp. 329–340.
[10] C. Lin, B. Henty, R. Cooper, D. D. Stancil, and B. Fan, "A Measurement Study of time-scaled 802.11a waveforms over the mobile-to-mobile vehicular channel at 5.9 GHz," *IEEE Commun. Mag.*, vol. 46, no. 5, pp. 84–91, May 2008.
[11] J. Hagenauer, "Rate-compatible punctured convolutional codes (RCPC codes) and their applications," *IEEE Trans. Commun.*, vol. 36, no. 4, pp. 389–400, Apr. 1988.
[12] S. Kallel, "Complementary punctured convolutional (CPC) codes and their applications," *IEEE Trans. Commun.*, vol. 43, no. 6, pp. 2005–2009, Jun. 1995.
[13] U. Dammer, E. Naroska, S. Schmermbeck, and U. Schwiegelshohn, "A data puncturing IR-scheme for type-II hybrid ARQ protocols using LDPC codes," in *Proc. IEEE GLOBECOM*, Dallas, TX, USA, Dec. 2004, pp. 3012–3016.
[14] S. Sesia, G. Caire, and G. Vivier, "Incremental redundancy hybrid ARQ schemes based on low-density parity-check codes," *IEEE Trans. Commun.*, vol. 52, no. 8, pp. 1311–1321, Aug. 2004.
[15] S. Kallel, R. Link, and S. Bakhtiyari, "Throughput performance of memory ARQ schemes," *IEEE Trans. Veh. Technol.*, vol. 48, no. 3, pp. 891–899, May 1999.
[16] K. Akhavan, S. Farahvash, and M. Kavehrad, "Performance of hybrid ARQ schemes with ML code combining over a block-fading Rayleigh channel," *Int. J. Wireless Inf. Netw.*, vol. 7, no. 1, pp. 1–8, Jan. 2000.
[17] H. Boujemâa, "Delay analysis of cooperative truncated HARQ with opportunistic relaying," *IEEE Trans. Veh. Technol.*, vol. 58, no. 9, pp. 4795–4804, Nov. 2009.

[18] G. Caire and D. Tuninetti, "The throughput of hybrid-ARQ protocols for the Gaussian collision channel," *IEEE Trans. Inf. Theory*, vol. 47, no. 5, pp. 1971–1988, Jul. 2001.

[19] B. Maham, A. Behnad, and M. Debbah, "Analysis of outage probability and throughput for half-duplex hybrid-ARQ relay channels," *IEEE Trans. Veh. Technol.*, vol. 61, no. 7, pp. 3061–3070, Sep. 2012.

[20] P. Wu and N. Jindal, "Performance of hybrid-ARQ in block-fading channels: A fixed outage probability analysis," *IEEE Trans. Commun.*, vol. 58, no. 4, pp. 1129–1141, Apr. 2010.

[21] A. Chelli and M. Pätzold, "On the performance of hybrid-ARQ with code combining over double Rayleigh fading channels," in *Proc. IEEE 22nd Symp. PIMRC*, Toronto, ON, Canada, Sep. 2011, pp. 2014–2019.

[22] A. Chelli, J. R. Barry, and M. Pätzold, "Performance of hybrid-ARQ with incremental redundancy over double Rayleigh fading channels," in *Proc. IEEE 73rd Veh. Technol. Conf. (VTC-Spring)*, Budapest, Hungary, May 2011, pp. 1–6.

[23] M. Abramowitz and I. A. Stegun, *Handbook of Mathematical Functions: With Formulas, Graphs, and Mathematical Tables*. New York, NY, USA: Dover, 1964.

[24] W. Rui and V. Lau, "Combined cross-layer design and HARQ for multiuser systems with outdated channel state information at transmitter (CSIT) in slow fading channels," *IEEE Trans. Wireless Commun.*, vol. 7, no. 7, pp. 2771–2777, Jul. 2008.

[25] S. Verdú and T. S. Han, "A general formula for channel capacity," *IEEE Trans. Inf. Theory*, vol. 40, no. 4, pp. 1147–1157, Jul. 1994.

[26] W. Chan, T.-C. Lu, and R.-J. Chen, "Pollaczek-Khinchin formula for the M/G/1 queue in discrete time with vacations," *Proc. Inst. Elect. Eng—Comput. Digital Tech.*, vol. 144, no. 4, pp. 222–226, Jul. 1997.

[27] J. Choi and D. To, "Energy efficiency of HARQ-IR for two-way relay systems with network coding," in *Proc. 18th EW*, Poznań, Poland, Apr. 2012, pp. 1–5.

[28] C. Li, S. H. Song, J. Zhang, and K. B. Letaief, "Maximizing energy efficiency in wireless networks with a minimum average throughput requirement," in *Proc. IEEE WCNC*, Paris, France, Apr. 2012, pp. 1130–1134.

[29] G. Y. Li *et al.*, "Energy-efficient wireless communications: Tutorial, survey, and open issues," *IEEE Trans. Wireless Commun.*, vol. 18, no. 6, pp. 28–35, Jul. 2011.

[30] H. J. Greenberg and W. P. Pierskalla (1971, Nov./Dec.). A review of quasi-convex functions. *Oper. Res.* [Online]. *19(7)*, pp. 1553–1570. Available: http://www.jstor.org/stable/169178

[31] S. Boyd and L. Vandenberghe, *Convex Optimization*. Cambridge, U.K.: Cambridge Univ. Press, 2004.

[32] L. Zheng and D. Tse, "Diversity and multiplexing: A fundamental tradeoff in multiple-antenna channels," *IEEE Trans. Inf. Theory*, vol. 49, no. 5, pp. 1073–1096, May 2003.

[33] H. El-Gamal, G. Caire, and M.-O. Damen, "The MIMO ARQ channel: Diversity-multiplexing-delay tradeoff," *IEEE Trans. Inf. Theory*, vol. 52, no. 8, pp. 3601–3621, Aug. 2006.

[34] S. Primak, V. Kontorovitch, and V. Lyandres, *Stochastic Methods and Their Applications to Communications: Stochastic Differential Equations Approach*. Hoboken, NJ, USA: Wiley, 2004.

[35] Y. L. Luke, *The Special Functions and Their Approximations.* New York, NY, USA: Academic, 1969.

[36] Wolfram Research, *Mathematica Edition: Version 8.0*, Champaign, IL, USA, Wolfram Res., 2010.

[37] J. Salo, H. M. El-Sallabi, and P. Vainikainen, "The distribution of the product of independent Rayleigh random variables," *IEEE Trans. Antennas Propag.*, vol. 54, no. 2, pp. 639–643, Feb. 2006.

Emna Zedini was born in Beja, Tunisia. She received the B.Sc. and M.Sc. degrees in communications from Ecole Superieure des Communications de Tunis (SUP'COM), Tunis, Tunisia, in 2010 and 2011, respectively. Currently, she is pursuing the Ph.D. degree in electrical engineering at King Abdullah University of Science and Technology (KAUST), Thuwal, Makkah Province, Saudi Arabia. Her main research interests are in modeling and performance analysis of optical wireless communication systems.

Mohamed-Slim Alouini (S'94–M'98–SM'03–F'09) was born in Tunis, Tunisia. He received the Ph.D. degree in electrical engineering from the California Institute of Technology (Caltech), Pasadena, CA, USA, in 1998. He served as a faculty member at the University of Minnesota, Minneapolis, MN, USA, then at Texas A&M University at Qatar, Education City, Doha, Qatar, before joining King Abdullah University of Science and Technology (KAUST), Thuwal, Makkah Province, Saudi Arabia as a Professor of electrical engineering in 2009. His current research interests include the modeling, design, and performance analysis of wireless communication systems.

John R. Barry (SM'14) received the B.S. degree (summa cum laude) from the State University of New York at Buffalo in 1986, and the M.S. and Ph.D. degrees from the University of California at Berkeley in 1987 and 1992, respectively, all in electrical engineering. His doctoral research explored the feasibility of broadband wireless communications using diffuse infrared radiation. Since 1985, he has held engineering positions in the fields of communications and radar systems at Bell Communications Research, IBM T.J. Watson Research Center, Hughes Aircraft Company, and General Dynamics. He is a coauthor of *Digital Communications* (Kluwer, 2004), a co-editor of *Advanced Optical Wireless Communications Systems* (Cambridge Univ. Press, April 2012), and the author of *Wireless Infrared Communications* (Kluwer, 1994). He received the 1992 David J. Griep Memorial Prize and the 1993 Eliahu Jury Award from U.C. Berkeley and a 1993 IBM Faculty Development Award. He is currently serving as Technical Program Chair for IEEE Globecom 2013.

Ali Chelli (S'08–M'12) was born in Sfax, Tunisia. He received the B.Sc. degree in communications from Ecole Superieure des Communications de Tunis (SUP'COM), Tunis, Tunisia, in 2005. He received the M.Sc. degree in information and communication technology from University of Agder, Norway, in 2007. He received the Ph.D degree in information and communication technology from University of Agder, Norway, in 2013. He served as a Postdoctoral Fellow at King Abdullah University of Science and Technology (KAUST). Currently, he is a Researcher at the University of Agder, Norway. His research interests include wireless communication theory with focus on performance analysis of cooperative relaying, vehicle-to-vehicle communications, game theory, and channel modelling.

Matthias Pätzold (SM'98) received the Dipl.-Ing. and Dr.-Ing. degrees in electrical engineering from Ruhr-University Bochum, Bochum, Germany, in 1985 and 1989, respectively, and the habil. degree in communications engineering from the Technical University of Hamburg-Harburg, Germany, in 1998. From 1990 to 1992, he was with ANT Nachrichtentechnik GmbH, Backnang, Germany, where he was engaged in digital satellite communications. From 1992 to 2001, he was with the department of digital networks at the Technical University Hamburg-Harburg. Since 2001, he has been a full professor of mobile communications with the University of Agder, Norway. He authored several books, book chapters, and more than 250 technical papers. His publications received 13 best paper awards. He has been actively participating in numerous conferences serving as TPC chair and TPC member.